Hard X-Ray Photon Correlation Spectroscopy Methods for Materials Studies*

Alec R. Sandy,[1] Qingteng Zhang,[1] and Laurence B. Lurio[2] [1]X-Ray Science Division, Argonne National Laboratory, Lemont, Illinois, USA, 60439; email: asandy@anl.gov [2]Department of Physics, Northern Illinois University, DeKalb, Illinois, USA, 60115; email: llurio@niu.edu

Abstract

Understanding and designing sophisticated new materials requires measurements of not only their average structural properties but also their dynamic behavior. X-ray photon correlation spectroscopy (XPCS) provides this information by characterizing fluctuations in condensed matter across a broad range of length and time scales. Over the past two decades XPCS has provided a wide variety of results in the study of material properties. In this review, we provide an overview of coherence, photon correlation spectroscopy and the dynamic structure factor as well as information on the mechanics of XPCS experiments. We highlight the impact that this infrastructure has had on materials research and the bright future that is forthcoming with the anticipated upgrade of many third generation synchrotron sources to fourth generation multi-bend achromat sources.

CONTENTS

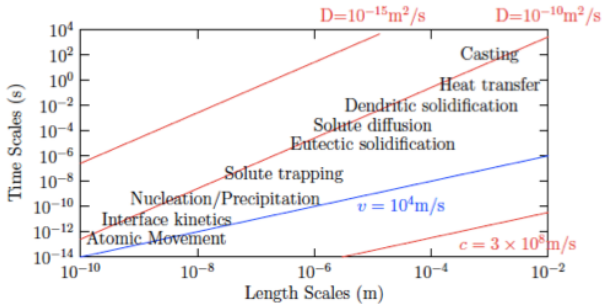

FIG. 1. Map of time and length scales in condensed matter science. XPCS provides information about many of these material processes. Figure from a talk by Prof. Nik Provatas, Department of Physics, McGill University.

I. INTRODUCTION

Understanding and creating new materials increasingly requires measurements of not only the time-averaged or instantaneous properties of the material but also its kinetic and dynamic behavior. Photon correlation spectroscopy (PCS) provides this information by characterizing fluctuations in condensed matter across a broad range of length and time scales while x-ray scattering provides sensitivity to order and motion at scales as small as the atomic scale. The combination of these techniques, XPCS, provides such information at the nanoscale and below. As illustrated by the schematic in Fig. 1, the spatiotemporal range provided by XPCS today and in the future with the ongoing development of diffraction-limited storage rings will enable studies of nucleation and precipitation and growth, coarsening, eutectic solidification and spinodal decomposition, de-alloying, de-wetting, solute trapping, dendritic solidification, electromigration and many other processes that are vital for understanding fundamentals of materials phase transformation and crucial for a wide range of materials processing and synthesis. Fluctuations are expected to play a crucial role in many of these processes, while at the same time, the spontaneous nature by which these processes begin, their non-equilibrium nature and the wide range of time- and length-scales makes these systems ideally suited for studies using time-resolved coherent x-ray methods like XPCS.

Figure 2 summarizes phase space accessible to various wave-vector and frequency-resolved measurement techniques. In principle, XPCS encompasses the lower right portion of this phase space. but the practical reach to-date has been considerably less than illustrated

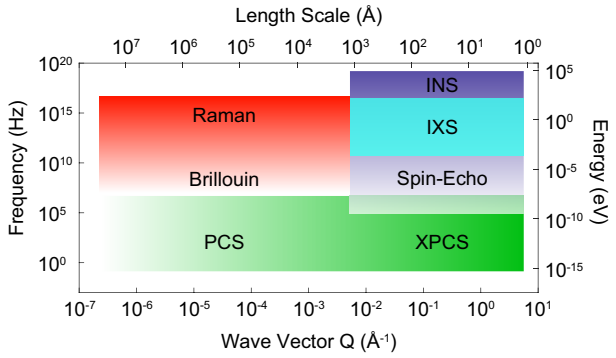

FIG. 2. Phase space accessible to XPCS and other wave-vector and frequency-resolved experiment techniques. PCS = (laser) photon correlation spectroscopy, INS = inelastic neutron scattering and IXS = inelastic x-ray scattering.

because of limited source brightness and detector capabilities. The advent of so-called multi-bend achromat (MBA) devices promises to dramatically improve this situation and broaden the scope of XPCS-enabled studies of materials.

XPCS measures spontaneous density fluctuations, i.e., heterogeneity, within a material at equilibrium. This cannot be done with conventional x-ray scattering since an incoherent x-ray beam only measures the ensemble-averaged density correlation function. In equilibrium, this function does not change and is therefore insensitive to fluctuations. In the case of x-ray scattering using a coherent beam, the coarse grained (smoothed) scattering pattern is the same as for incoherent scattering. At a fine-grained level, however, large intensity fluctuations appear. These fluctuations are known as speckle. A representative scattering pattern from an Fe_3Al superlattice illustrating speckle is shown in Fig. 3. For a fully coherent beam, the speckle intensity varies from zero to twice the average intensity. A snapshot of the scattering pattern shows fine spatial variations while for a dynamic sample a time series from a particular point in reciprocal space will show intensity fluctuations versus time. The persistence time of a speckle at a particular wavevector, $\vec{Q}$, is related to the relaxation time of density fluctuations in the sample at the length scale corresponding to that wavevector.

In the remainder of this review, we provide an introduction to coherence, photon correlation spectroscopy and the dynamic structure factor along with the practicalities of such experiments. The discussion includes examples of the these methods applied to understanding materials and materials formation stability across a broad spectrum of condensed matter that spans soft colloidal suspensions to quantum solids. We end with a brief discussion of

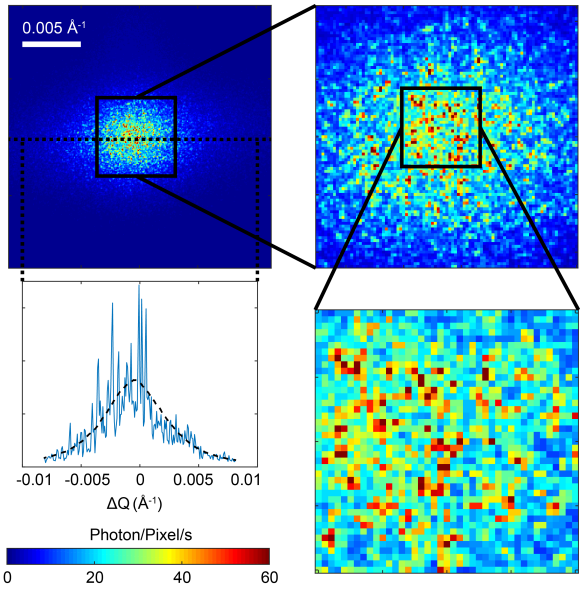

FIG. 3. Speckled scattering from the $(\frac{1}{2}\ \frac{1}{2}\ \frac{1}{2})$ superlattice peak of a quenched Fe_3Al sample. Clockwise from upper left: 2-D scattering pattern, zoom-in of the 2-D scattering pattern, further zoom-in and cross-section of the scattering pattern plotted above. In the lower left panel the thin solid line is a cross-section (dashed horizontal line in the top left panel) through the scattering peak while the dashed line is a smooth guide-to-the-eye. The fine features in these figures are speckle.

future prospects for XPCS that are especially promising because of the advent of fourth generation, near-diffraction-limited multi-bend achromat (MBA) sources that will provide coherent fluxes many times higher than today. We note that there have been several excellent XPCS reviews in recent years—see Refs. [1]–[6]—a goal of this review is to complement those by providing a more materials-related focus.

II. COHERENT X-RAY SCATTERING AND XPCS

A. Coherence

The primary distinction between performing an x-ray scattering experiment with a coherent beam versus an incoherent beam is that in the far-field, the speckled scattering pattern produced by a coherent x-ray beam provides information about the exact structure of a material while an incoherent beam does not. Since the first coherent x-ray scattering demonstration in 1991 [7], such measurements have largely developed in two different

directions. First, a wealth of phase inversion or lensless imaging techniques have been developed with the goal of determining the exact structure of materials at a particular time [8]. Second, dynamics measurements, employing XPCS, have focused on understanding the statistical properties of exact structural changes in materials. Intense coherent x-ray beams are required for both techniques. In the rest of this section we summarize coherence as it pertains to performing XPCS experiments.

A detailed discussion of optical coherence can be found in standard textbooks on optics [9], [10]. There are two aspects of coherence: (1) transverse and (2) longitudinal or temporal coherence. Transverse coherence is the maximum lateral distance between two scatterers that still creates an interference pattern at a distant detector while longitudinal coherence is the allowed wavelength spread that still results in an interference pattern. In either case, the intensity of the scattered radiation measured at a distant detector shows an interference pattern that arises from the path length difference of radiation from different scattering elements. A coherent scattering pattern like that shown in Figure 3, can be characterized by its visibility or contrast defined by

$$V = 2(I_{\max} - I_{\min})/(I_{\max} + I_{\min}). \tag{1}$$

This is unity in the case of coherent radiation and decreases to zero for an incoherent beam. If the source of the incident wave is a monochromatic point source, all wavefronts will be fully coherent. When the source has finite spatial extent, the visibility of the interference pattern will depend on the separation of the scatterers. The interference pattern will begin to fade when the spacing between the scatterers exceeds the transverse coherence length, ξ, which is inversely related to the size of the source. When the source has finite bandwidth, then the interference pattern will also begin to fade when the time delay between the two wavefronts exceeds the correlation time Λ/c where Λ is the longitudinal coherence length. Together these quantities determine a coherence volume. A necessary condition for performing XPCS measurements is that the scattering volume of the sample does not greatly exceed the coherence volume.

X-ray source sizes at synchrotrons (undulator source points) can usually be represented by a Gaussian intensity distribution [11] characterized by the second moments σ_x and σ_y, with x horizontal and y vertical. The transverse coherence lengths are given by [12]

$$\xi_{x,y} = \lambda R/2\pi\sigma_{x,y}, \tag{2}$$

where λ is the x-ray wavelength and R is the distance from the source to the sample. Typical numbers at an early third generation source like the Advanced Photon Source (APS) at Argonne National Laboratory are $\sigma_x = 270$ μm and $\sigma_y = 10$ μm. With $R = 65$ m and $\lambda = 1.1$ Å the transverse coherence lengths are $\xi_x = 4$ μm and $\xi_y = 120$ μm.

The longitudinal coherence length is defined by [13]

$$\Lambda = E^2/\Delta E, \tag{3}$$

where ΔE is the full-width-at-half-maximum (FWHM) of the energy spectrum. For a Si(111) monochromator the bandpass is $\sim 10^{-4}$ so for $\lambda = 1.1$ Å, $\Lambda \approx 1.1$ μm. This limits sample thicknesses or penetration depths to ≈ 1 μm in the case of wide angle scattering.

B. Time Correlation Functions

If the distribution of matter or disorder within a sample fluctuates in time, the x-ray speckle pattern generated by coherent scattering from the sample will also fluctuate. XPCS relates fluctuations in the speckle pattern to the dynamics within the sample via the intensity-intensity correlation function. The intensity-intensity correlation function is defined by

$$G_2(\vec{Q}, t) = \left\langle I\left(\vec{Q}, t'\right) I\left(\vec{Q}, t' + t\right)\right\rangle_{t'}. \tag{4}$$

This quantity is known as G_2 because it correlates intensities, I, which are the square of the electric field. G_2 is typically normalized by the square of the average intensity to give the quantity called g_2:

$$g_2(\vec{Q}, t) = \frac{\left\langle I\left(\vec{Q}, t'\right) I\left(\vec{Q}, t' + t\right)\right\rangle}{\left\langle I\left(\vec{Q}\right)\right\rangle^2}. \tag{5}$$

The averages implied by <> can either be averages over time or averages over speckles at equivalent values of $\vec{Q}$ or both.

C. The Dynamic Structure Factor

The dynamic structure factor, known as g_2, is a function of the electric field intensity distribution at the detector via

$$g_2(\vec{Q}, t) = \frac{1}{I^2} \int_{V'} e^{i\vec{Q}\cdot\vec{r}'} \left\langle E^2(\vec{r}, t') E^2(\vec{r} + \vec{r}', t' + t)\right\rangle_{\vec{r}', t'} d^3r', \tag{6}$$

with $I = \langle E^2 \rangle$. This is a fourth order correlation function in the electric fields. It can be reduced to a product of second order correlation functions via the Van Cittert-Zernike theorem:

$$g_2(\vec{Q}, t) = 1 + \beta \left\langle E(\vec{Q}, 0) E(\vec{Q}, t) \right\rangle^2 / I^2, \tag{7}$$

where β is the optical contrast. This second order electric field correlation function is related to the dynamic structure factor of the material.

$$\left\langle E(\vec{Q}, 0) E(\vec{Q}, t) \right\rangle^2 / I^2 = F(\vec{Q}, t)/F(\vec{Q}, 0) = f(\vec{Q}, t), \tag{8}$$

where

$$F(\vec{Q}, t) = \int_V e^{i\vec{Q}\cdot\vec{r}} \langle \rho(0, 0), \rho(\vec{r}, t) \rangle \, d^3\vec{r}, \tag{9}$$

which is the Fourier transform of the charge-density correlation function of the material. Equations 8 and 9 lead to the central relationship between the measured time correlation function and the sample dynamics:

$$g_2(\vec{Q}, t) = 1 + \beta f(\vec{Q}, t)^2. \tag{10}$$

Thus, a determination of the time correlation function through XPCS provides the intermediate scattering function (ISF), often called g_1, of a material. The ISF provides a measure of density fluctuations within a material. In particular, the fluctuation-dissipation theorem relates the spectrum of spontaneous thermal fluctuations to the susceptibility, $\chi(t)$, of the material to an external force, $S(\vec{k}, \omega) = (2k_B T/\omega)\mathrm{Im}\left[\hat{\chi}(\vec{k}, \omega)\right]$ [14], where k_B is the Boltzmann constant, T is the temperature, ω is the frequency, $\vec{k}$ is the wavevector and $\mathrm{Im}[\hat{\chi}]$ is the imaginary part of the Fourier transform of $\chi(t)$. Knowledge of the dynamic structure factor provides information about how a material responds to perturbations close to equilibrium and can also provide connections with theoretical calculations of material properties. This information has applications in areas such as understanding Brownian motion and diffusive behavior, fluctuations of surfaces and membranes, density fluctuations, order-disorder fluctuations, concentration fluctuations in binary fluids and atomic lattice position fluctuations.

III. XPCS PRACTICALITIES

A. XPCS Facilities

XPCS capabilities depend strongly on the brilliance, B, of the source. Though there were important coherent scattering achievements at second generation sources like the National Synchrotron Light Source (NSLS), i.e., [7], [15], considerably more brilliance like that provided by third generation sources and FELs is required to make XPCS scattering experiments practical. This section summarizes the capabilities at beamline 8-ID at the APS as an example of a typical XPCS facility; other dedicated synchrotron XPCS facilities exist at the ESRF in Grenoble, France; Petra-III in Hamburg, Germany; and NSLS-II in Upton, New York, USA.

Wide-angle XPCS (WA-XPCS) is well suited for studying hard condensed matter such as alloys and atomic glasses; at the APS this set-up is housed in enclosure 8-ID-E [16]. The set-up contains transverse coherence-length selecting slits, a CRL for 1-D vertical focusing at the sample position and a small multi-circle diffractometer with a 1 m exit flight path. A CCD area detector collects speckle patterns over a small solid angle. For coherence-selecting slit apertures of 150 μm (vertical) and 10 μm (horizontal), the flux at the sample position is 3×10^9 ph/s at a fixed x-ray energy of 7.35 keV. This set-up has been used for a variety of materials-relevant work over recent years including measurements of the spontaneous fluctuations of ferroelectric domains in a ferroelectric-dielectric superlattice [17], domain boundary fluctuations in multi-ferroics [18], pinned and fluctuating charge-density waves in Cr thin films [19], bulk Cr [20] and 1T-TaS_2 [21], fluctuations and avalanches in metals and metal alloys [22]–[24] and step migration and surface re-arrangements on clean metals and metals under electrochemical conditions [25]–[30].

Small-angle XPCS (SA-XPCS) is performed in enclosure 8-ID-I. The layout is shown schematically in Fig. 4. From right-to-left, 8-ID-I contains transverse coherence-length selecting slits, a CRL for 1-D vertical focusing at the sample position, a sample platform capable of supporting a wide variety of sample environments, a 4.5-m-long exit flight path and a variety of area detectors. For coherence-selecting slit apertures of 150 μm (vertical) and 20 μm (horizontal), the focused flux at the sample position is 7×10^{10} ph/s at the most typical operating energy of 11 keV. One rich area of investigation at 8-ID-I is

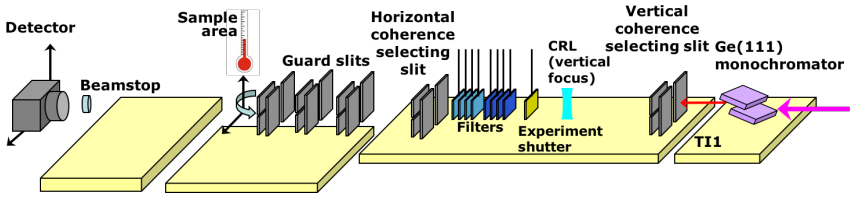

FIG. 4. Schematic of the small-angle XPCS setup at 8-ID-I at the Advanced Photon Source. The monochromator is 65 m from the source and the sample area is 68 m from the source. The detector and beamstop are 4 m downstream of the sample area.

nanoparticle-polymer blends since such materials offer the promise of optimized electrical, optical or mechanical properties in flexible composites [31]–[51].

B. Detectors for XPCS

What can be learned about materials using XPCS is dictated not only by the x-ray source brightness but also by relevant detector capabilities. Because signal levels are low, XPCS detectors must be able to record small numbers of scattered photons with high fidelity and relatively high spatial resolution is required to resolve x-ray speckle patterns. In addition, higher frame rates provide a wider dynamic range for studying fluctuations and kinetics in materials. The best commercial XPCS area detectors right now are pixel array detectors (PADs) supplied by either Dectris or X-Spectrum. PADs use a sensor bump-bonded to a readout chip. The Pilatus detector [52] developed at the Paul-Scherrer Institute was the first widespread detector of this sort and it has made extensive inroads in the x-ray scattering community but the pixel size of 172 μm is generally too large for XPCS and the highest frame rates are also less than desired. Since the development of the Pilatus, several other PADs have been developed with pixel sizes and frame rates more applicable to XPCS. These include the Dectris Eiger [53] with 75-μm pixels and narrow-dynamic-range 0.5-megapixel frame rates up to 9,000 frames per second (fps), and the X-Spectrum Lambda [54] with 55-μm pixels and anticipated narrow-dynamic-range 0.75-megapixel frame rates up to 24,000 fps.

IV. XPCS TO PROBE MATERIAL STABILITY AND STRENGTHENING

A. Structural Arrest in Silica Colloids

Understanding the dynamic properties and stability of amorphous materials is important because of their existing and anticipated technological applications. For instance, bulk metallic glasses (BMGs) are an important class of materials in this family [55]–[57] and exhibit solid-like behavior with liquid-like order. A key advantage of BMGs is that their low critical cooling rates allow, as their name suggests, the production of bulk samples in quantities facilitating cost-effective and scalable applications. Another advantage is thermoplastic-like deformability in their super-cooled state allowing production of defect-free precision shapes spanning length scales from the nano- to macro-scale. Understanding the glass transition and the more general problem of structural arrest in materials like these is of considerable interest [58], [59] to facilitate rational design and control of their properties. To date, XPCS studies of the dynamic properties of actual metallic glasses have been extremely challenging because of low scattering signals and largely await the emergence of nascent 4^{th} storage ring light sources such as ESRF-EBS and APS-U though there have been some notable successes in this area [60]–[63]. In an effort to better understand the dynamic properties of amorphous materials many groups have studied analogs composed of colloidal nanoparticles[15], [36], [64]–[79].

Colloidal suspensions also provide the most readily understood example of relating the dynamic structure factor of a material to its observed dynamics or correlation functions. As an example, we consider the Brownian diffusion of a dilute colloidal suspension. Suppose that there are N particles suspended in a fluid of viscosity η located at positions $\vec{r}_i$. The dynamic structure factor of this system is given by

$$f(\vec{Q},t) = \left\langle \frac{1}{N}\sum_{i,j} e^{i\vec{Q}\cdot[\vec{r}_i(0)-\vec{r}_j(t)]} \right\rangle \tag{11}$$

We assume the particle motions are uncorrelated. In this case, the terms with $i \neq j$ drop out giving;

$$f(\vec{Q},t) = \left\langle \frac{1}{N}\sum_{i,j} e^{i\vec{Q}\cdot[\vec{r}_i(0)-\vec{r}_i(t)]} \right\rangle = \left\langle e^{i\vec{Q}\cdot\Delta r(t)} \right\rangle = e^{-\frac{1}{2}\left\langle \vec{Q}\cdot\vec{\Delta}r(t)\right\rangle^2}. \tag{12}$$

For a non-interacting solution of diffusing particles $\left\langle \vec{Q} \cdot \vec{\Delta r}(t) \right\rangle^2 = 2QDt$. We then obtain:

$$f(\vec{Q}, t) = f(Q, t) = e^{-DQ^2 t}. \tag{13}$$

The correlation time, τ, is the time at which the argument of the exponential = 1 so $\tau = 1/DQ^2$ The diffusion constant D can be related to the solution viscosity, η, and the particle radius a through the Stokes-Einstein relationship: $D = k_B T/6\pi\eta a$.

The model of the ISF as a simple exponential decay related to the diffusion constant can also be generalized. The most straightforward generalization is that the diffusion constant can depend on length scale [80]. In this case one can fit the ISF to the generalized form $e^{-D(Q)t}$, with $D(Q)$ a length-scale-dependent diffusion constant. For systems such as dense colloids or polymer melts, one often finds that there is a fast decay and a slow decay of the ISF, related to caging effects [81], [82]. In these cases, the ISF can often be well described by a double exponential decay of the form $f(Q,t) = (1-\alpha)e^{-\Gamma_1 t} + \alpha e^{-\Gamma_2 t}$ with Γ_1 the short-time and Γ_2 the long-time decay constants. The short- and long-time decay constants can be related to the β- and α-decay times in a colloidal glass, for example [83]. In the case where there are multiple, overlapping relaxation times, the ISF can often be well fit using a stretched exponential of the form $e^{-(\Gamma t)^\nu}$ where ν is a stretching exponent. These various forms for the ISF will be illustrated in the examples given below.

As a more complicated example of colloidal dynamics, we consider the re-entrant glassy behavior exhibited by silica colloids in a water-lutidine mixture as a function of temperature when the solvent mixture is near its critical point. Water-lutidine mixtures undergo a demixing transition just above room temperature. As the temperature of the suspension is raised to near this temperature, silica colloids in such a mixture undergo reversible aggregation[84]. The first XPCS study of such a system [85] combined ultra-small-angle x-ray scattering and point-detector XPCS measurements on a volume fraction (ϕ) = 0.08 suspension of radius (R) = 60.4 nm silica particles in a binary mixture of 2,6 lutidine and heavy water. The system underwent reversible aggregation at a temperature $T_A = 26.805$ °C: below this temperature, the colloids exhibited fluid-like properties while above this temperature the results were indicative of jammed or frozen particle dynamics.

Subsequent work on a similar system [86], [87] applied a newly developed fast frame-rate area detector [88] to the problem. Lu *et al.* examined $\phi \approx 0.5$ volume fraction suspensions in near critical water-lutidine mixtures with a lutidine concentration of 0.24 and $R = 195$ nm.

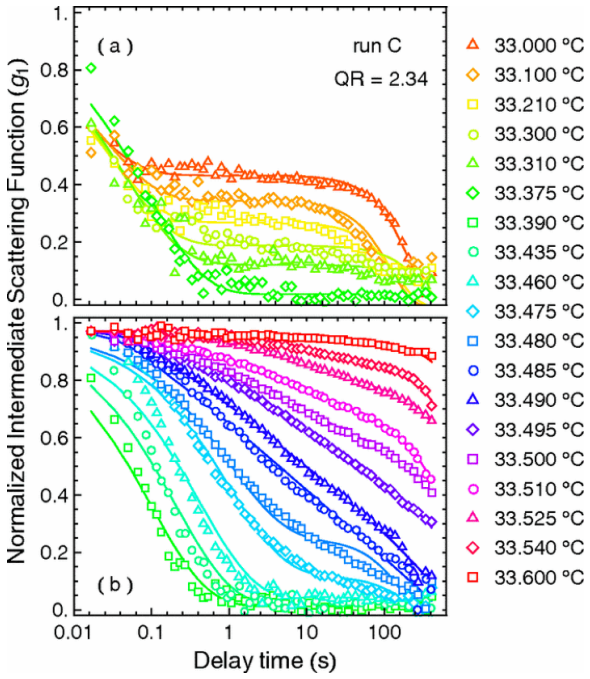

FIG. 5. Correlation functions as a function of temperature. The correlation functions were obtained from one sequence of measurements as the temperature was raised from 33.000 °C to 33.600 °C. Since the dynamics of the colloid suspension transition from arrested motion at lower temperature to more fluid-like motion at intermediate temperatures and then back to arrested motion at higher temperatures, the correlation functions have been separated into two panels so the changes are more visible. The top panel shows "melting" of the repulsive glass while the bottom panel shows "solidification" of the attractive glass. From Lu *et al.* [86].

For the parameters listed above, the suspension was in a regime where small changes in temperature varied the particle interactions through repulsive-glass (RG), liquid (L) and attractive-glass (AG) phases for small temperature changes. The fast area detector allowed the correlation functions to be calculated and, since the scattering was collected over nearly 2π in azimuth, $g_2 > 1$ could be determined even when the sample was effectively static. A sample series of correlation functions versus temperature (from Ref. [86]) are shown in Fig. 5. The correlation functions shown were obtained from a single temperature ramp in which temperature changed by only 0.6 °C. Panel (a) shows the RG phase and subsequent liquid-like dynamics as temperature is increased while (b) shows the emergence of the AG phase with fully-arrested dynamics. Particularly intriguing is the observation of logarithmic decays of the correlation functions [89] as the AG phase is approached from lower temperatures.

A key finding of this work relevant to this review is how only very small changes in a control parameter like temperature that produce only very modest changes in the structural properties of the material produce dramatically different dynamics or stability of the material that XPCS is sensitive to.

B. Strength of Polymer-Nanoparticle Composites

The addition of nanoparticles to a polymer can significantly modify the rheological or bulk mechanical properties of the material. XPCS measurements have the potential to reveal the microscopic mechanisms that cause these changes since they directly probe nanoparticle motion. Narayanan *et al.* [31] examined a system consisting of 26 nm alumina nanoparticles dispersed in poly-methyl-methacrylate (PMMA) of molecular weight 150 kg/mole. Bulk viscosity studies showed that the addition of nanoparticles led to a significant reduction in the glass transition temperature of the polymer. To investigate this effect they measured XPCS over a range of temperatures and nanoparticle concentrations. They found that the ISF could be fit using a stretched exponential of the form

$$f(q,t) = \exp\left[-\left(t/\tau_a\right)^{\beta}\right], \tag{14}$$

where τ_a represents the relaxation time and β is a stretching exponent. Their measured relaxation times and stretching exponents are shown in Fig. 6. At temperatures where the polymer was in the liquid regime but close to the glass temperature the stretching exponent was found to be less than unity, which could be interpreted in terms of multiple relaxation times within the material due to thermodynamic heterogeneity. Well above the glass transition temperature the exponents returned to $\beta = 1$ as expected for diffusion. Below the glass transition the exponent became greater than unity approaching a value close to $\beta = 1.5$, indicating faster than diffusive motion. In addition, below T_g the relaxation time τ_a was found to vary as $\tau_a \sim 1/Q$ unlike diffusive behavior where $\tau \sim 1/Q^2$. These characteristics had been observed previously in dynamic light scattering by Cipelletti *et al.* [90] for colloidal gels. The ballistic-like motion was interpreted as being driven by residual stress. Using a simple model of the stress as consisting of stress dipoles it could then be shown that this results in $\tau \sim 1/Q$ and $\beta = 1.5$. The model of Cipelletti *et al.* was expanded and put on a firmer theoretical basis by Bouchaud and Pitard [91]. Narayanan

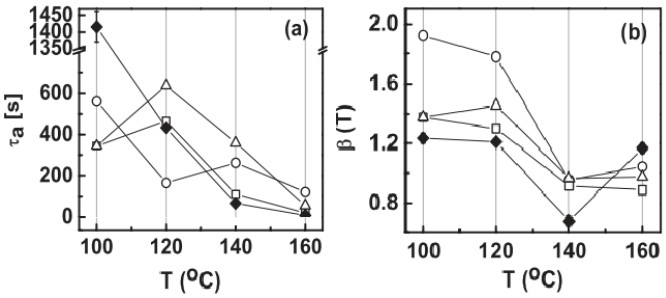

FIG. 6. Variation of the time constants and stretching exponents for alumina-PMMA nanocomposites vs. temperature. The different symbols indicate different weight percents of the alumina filler particles: circles are 0.1%, squares are 0.5% and diamonds are 5%. Data from Narayanan *et al.* [31].

et al. thus concluded that the glassy state was characterized by internal stress between the nanoparticles and polymer matrix which has implications for understanding the mechanical properties of these emerging important materials

Akcora *et al.* [92] examined a different nanocomposite system consisting of 14 nm diameter silica spheres with grafted polystyrene chains dispersed in a polystyrene matrix. They showed using TEM and ultra-small angle x-ray scattering (USAXS) that the morphology of the resulting composites could be tuned by varying the ratio of chain lengths of the grafted polymer to matrix polymer, and by varying the density of the grafted polymers. The particular question which they wanted to address was the mechanism by which the nanoparticles mechanically reinforce polymers. In particular, was the reinforcement optimized when the nanoparticles were evenly dispersed within the polymer, or when the nanoparticles formed connected networks within the polymer.

To study this question, they prepared two different samples, one with long grafted chains which dispersed uniformly within the fluid and a second with shorter grafted chains which aggregated into a morphology where the nanoparticles formed into thin sheets, which they called the connected sheet phase. Bulk rheology measurements indicated that at high concentrations the connected sheet phase showed more solid-like properties than the dispersed phase. XPCS measurements for nanoparticles in both phases could be fit with the stretched exponential form of Eq. 14. For both the connected sheet phase and the dispersed phase they found that the relaxation times scaled as $\tau_a \sim 1/Q$. For the connected sheet phase the stretching exponents were $\beta \sim 1.5$ (see Fig. 7) at high concentrations (15%) , and decreased

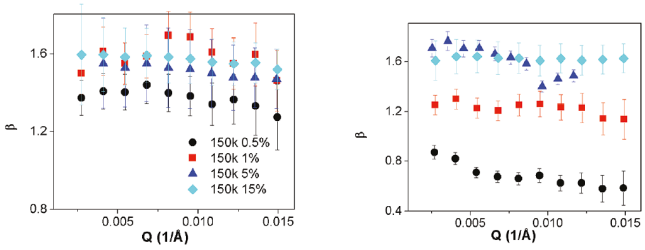

FIG. 7. Stretching exponents measured from silica-polystyrene composites. The left panel shows stretching exponents versus Q for nanoparticles in the connected sheet phase while the right panel shows stretching exponents for the dispersed phase. Data from Akcora *et al.* [92].

to $\beta \sim 1.3$ for lower concentrations (0.5%). This differed from the dispersed phase where the stretching exponent was 1.5 for the highest concentration, but decreased much more rapidly with concentration down to 0.5 for the 0.5% data. In some respects, this data is very similar to the glass phase data obtained by Narayanan *et al.* [31]. However, the dependence on the morphology of nanoparticle phase indicates that the ballistic motion does not result from a glassy polymer but rather the formation of a gel-like network formed by interacting nanoparticles within the polymer matrix. Strains within the gel drive the ballistic motions resulting in stretched exponential behavior with $\tau_q \sim 1/Q$ and $\beta = 1.5$. The dispersed nanoparticle phase has weaker networks and correspondingly less ballistic-like behavior. Akcora *et al.* also examined the aging of this material. They found that the velocity of the nanoparticles decreased by nearly a factor of 10 with annealing time over the course of 12 hours showing that stress within the gel network was slowly relaxing. An important result of this work was that the mechanical rigidity could be clearly identified with the interactions of nanoparticle networks within the polymer, indicating a pathway to tuning the polymer-nanoparticle interactions to engineer desired mechanical properties in composite materials.

C. Fluctuations of Nanoscale Charge and Spin Ordering in Quantum Materials

Spatial modulation of the electron density or spin orientation with a periodicity of only a few times of the interatomic spacing is found in many solid-state quantum materials. Some examples include charge density waves (CDWs) [93], spin density waves (SDWs) [94] and ferroelectric domains [17], [95]. Although the underlying atomic lattice is static, the spatially-modulated quantum structures can exhibit thermally induced spontaneous dynam-

ics at equilibrium. Understanding quantum fluctuations is one important aspect of ultimately designing and controlling such materials for novel applications; XPCS is one tool for observing such fluctuations.

Probing spontaneous quantum fluctuations with XPCS was first demonstrated by Shpyrko *et al.* [20] in the study of spontaneous dynamics in nm-wavelength SDWs in chromium. Elemental chromium has a body-centered cubic structure and is anti-ferromagnetic below 311 K. Three types of anti-ferromagnetic domains arise from sinusoidal modulation of spin orientations with a wavelength L of $6 \sim 8$ nm and a wavevector parallel to the three equivalent cubic (100) directions. The SDWs are coupled to CDWs and result in diffuse scattering intensities at the vicinity of lattice Bragg peaks. Fluctuations of the anti-ferromagnetic domain patterns are not observable with macroscopic probes but can be observed using XPCS.

As shown in Fig. 8(b), the intensity speckles produced by the exact CDW pattern evolve over time leading to a decay of the intensity correlation as shown in Fig. 8(a). The solid backwards triangles are the intensity speckles collected from the lattice Bragg peak and provide a stability reference. An intriguing observation is the overlap of dynamics measured at temperatures lower than 40 K. This deviation from the Arrhenius behavior indicates that the probability of a unit volume $(L/2)^3$ flipping from one domain type to another is dominated by quantum tunneling instead of thermal activation at very low temperatures. The important materials' insight provided by the observation of quantum fluctuation in chromium is that total decorrelation of spatial structures of the exact SDW arrangement occurs in a couple of hours even in the absence of significant thermal energy. As a result, stability engineering via pinning sites, for example, will be necessary for improving the retainability and repeatability of magnetic nanodomains for applications such as non-volatile memory [96] or domain wall logic gates [97].

V. XPCS FOR STUDIES OF MATERIALS FORMATION

A. Evolution of order in a quenched systems

While one of the chief strengths of XPCS is the ability to study fluctuations at equilibrium, it also has some unique advantages for the study of non-equilibrium systems. In particular,

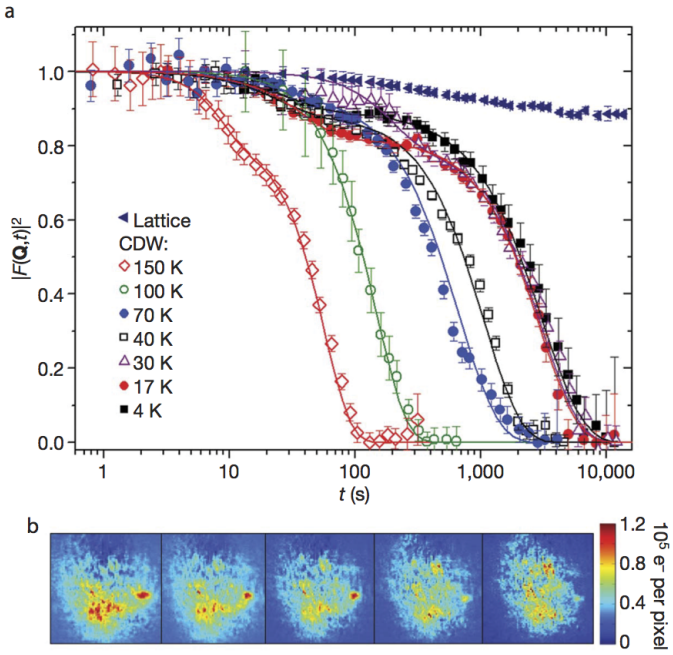

FIG. 8. (a) Decay of g_2 plotted as $|F(\mathbf{Q},t)|^2$ where $F(\mathbf{Q},t) = f(\vec{Q},t)$, showing CDW dynamics at different temperatures. Solid lines are empirical fits to the data. (b) Evolution of CDW speckle patterns at 17 K. The images span more than 10^{-2} Å^{-1} $\times$ 10^{-2} Å^{-1} in reciprocal space and are separated by in time by $\approx$ 1,000 s. From Shpyrko *et al.* [20].

material properties can depend in a sensitive way on domain formation that occurs during a quench. These domains, in turn, result from fluctuations about the non-equilibrium state during the quench. In order to study fluctuations about a non equilibrium state it is not possible to use the standard time correlation function $g_2(\vec{Q},t)$ since this is an equilibrium quantity, and does not depend on the particular time at which a measurement is made. Instead, non-equilibrium dynamics can be probed by using a two-time correlation function as was first done by Malik *et al.* [98]. There are various definitions of the two time correlation function that have been used in the literature and that can be shown to be equivalent [99]. One of the most common is given by

$$C\left(\vec{Q},t_1,t_2\right) = \left\langle D\left(\vec{Q},t_1\right) D\left(\vec{Q},t_2\right)\right\rangle. \tag{15}$$

The normalized intensity fluctuation, $D\left(\vec{Q},t\right)$, is defined by

$$D\left(\vec{Q},t\right) = \frac{I\left(\vec{Q},t\right) - \left\langle I\left(\vec{Q},t\right)\right\rangle}{\left\langle I\left(\vec{Q},t\right)\right\rangle}. \tag{16}$$

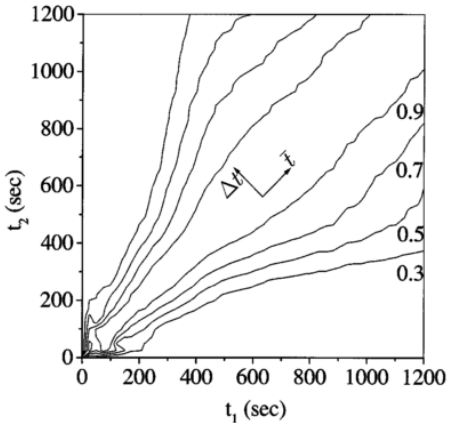

FIG. 9. Two time correlation function for phase separating borosilicate glass. from Malik *et al.* [98]

The averaging defined by $\left\langle I\left(\vec{Q},t\right)\right\rangle$ can obviously not be taken over time since $D\left(\vec{Q},t\right)$ is defined at a particular instant in time. If the system depends only on the magnitude of $\vec{Q}$ then the average intensity can be obtained from a circular average around a ring of scattering at constant Q. In more complicated cases the data is typically fit to a functional form which is smooth over the angular size of a speckle and the intensity at each point is then taken from the smoothed result.

Malik *et al.* [98] employed this method to study the formation of domains in sodium borosilicate glass. At high temperatures the glass is in a uniform phase, but when quenched to lower temperatures it phase separates into a B_2O_3-rich phase and a SiO_2-rich phase. The two-time correlation function for this system after a quench is shown in Fig. 9. For equilibrium fluctuations the dynamics would be constant in time, resulting in a uniform width of the diagonal cuts across the two-time correlation function. Instead, the width of these cuts (indicated by Δt in the figure) increase with absolute time from the quench. A more detailed analysis of the shape of the two-time function allowed them to extract the persistence time of speckles and indicated that the speckles persisted for a relatively long time during the quench so that structures formed in the material by spontaneous fluctuations early in the quench have a significant effect on the later domain shapes.

Fluerasu *et al.* [22] looked at domain coarsening after a quench for the metal alloy Cu_3Au. In the case of Cu_3Au the high temperature state has Cu and Au occupying random lattice sites in an FCC lattice. In the quenched state the Cu and Au order, with the Cu on the face

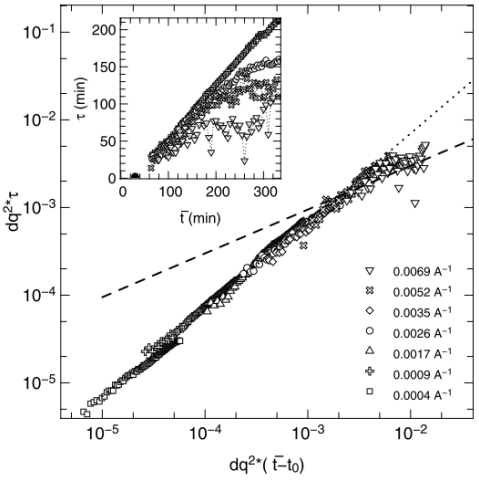

FIG. 10. Scaled relaxation time obtained from two-time correlation function for Cu_3Au after a quench as a function of scaled absolute time from the quench. The variable dq represents the distance from the center of the scattering peak, $\bar{t}$ the time since quench and t_0 is an offset time. From Fluerasu *et al.* [22].

sites and the Au on the corner sites. This system differs in a significant way from the case of borosilicate glass. For borosilicate glass, the order parameter (representing the density of boron) is conserved, while for Cu_3Au, the order parameter (representing the relative occupancy of the lattice sites) is not. Fluerasu *et al.* showed that for a non-conserved order parameter the relaxation time τ scales differently with the absolute quench time. They found $\tau \sim (\bar{t})^{\frac{1}{2}}$ at short times and $\tau \sim \bar{t}$ at long times (see Fig. 10) in agreement with theoretical expectations.

Sanborn *et al.* [23] used two-time correlation functions to examine the martensitic phase transition in cobalt. Cobalt undergoes a martensitic transition from a fcc phase above 720 °C to a hcp phase at lower temperatures. The two time correlation function measured after a quench through the martensitic transition is shown in Fig. 11. This two-time function is strikingly different from those obtained from the previous two cases. Instead of a continuous evolution, the correlation function exhibits discontinuous jumps where the scattering after the jump is completely uncorrelated with the earlier scattering. They interpret this as resulting from avalanches occurring in the cobalt as the hcp phase re-arranges to relieve stress. Analysis of the avalanches allows them characterize the number of avalanche events, N, as a function of the size of the avalanche, A. They then show that $N(A) \sim A^{-\alpha}$ with

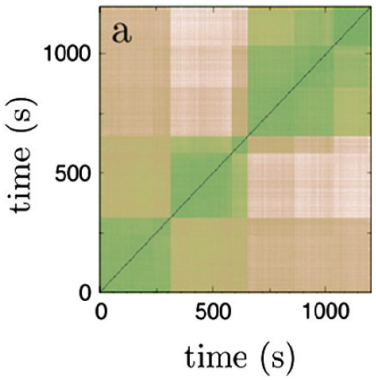

FIG. 11. Two time correlation function from the martensitic transition in cobalt. Discontinuities in the time correlation function are avalanche events corresponding to stress relief events in the hcp phase. From Sanborn *et al.* [23].

$\alpha = 1.7 \pm 0.2$. Interestingly, the statistics of these avalanches shows similarities to the statistics of earthquakes and have relevance to understanding the long-time stability and aging behavior of materials.

B. Gel Formation

Gels are fascinating materials with a wide variety of applications in consumer items such as pharmaceuticals, foods and personal care products. Understanding and ultimately controlling gelation, the process by which gels form, is a challenging scientific problem because during gelation, the gel-forming constituents form a system spanning network and the storage modulus of the material changes by several orders of magnitude [100]. Gels formed of colloidal nanoparticles are one particularly well studied system because aspects of their behavior can be explored through readily variable properties like particle size and coating, for example [101]. A colloidal gel is formed when particles suspended in solution become unstable to aggregation, ultimately forming a network that imparts mechanical rigidity to the system. The time required for this process can vary from a fraction of a second to many hours depending on the concentration of the particles and the strength of their attraction for one another. This sensitivity creates a scientific challenge that is central to the field of soft matter but also an opportunity for designing materials with properties tailored for specific applications. XPCS, especially when combined with macroscale-sensitive

rheology measurements, provides insight into how changes in the bulk properties of a gel-forming material change during gelation and how these changes correlate with changes in the nanoscale structure and dynamics of the constituents.

A recent example of work in this area was observing the later time formation of intermediate concentration colloidal gels after a temperature quench from a higher temperature fluidized state to a lower temperature gel-forming state [71]. The study found that after the quench there was prolonged latency period in which the suspension remains fluid before acquiring a significant shear modulus. At the nanoscale, XPCS revealed that the particles become increasingly localized during the latency period. At longer time scales after the quench, XPCS revealed slow hyper-diffusive motion of the nanoparticles that corresponds to the release of strain in the system.

More recently, an improved, i.e., faster, XPCS area detector [102], [103] has allowed a more sensitive probe of the nanoscale gel dynamics much earlier in the gel formation process [104]. Coherent scattering patterns collected by the UFXC were used to measure the autocorrelation decay functions of a gel-forming nanoparticle suspension as a function of time after it had been quenched into the gel-forming regime. Figure 12 shows autocorrelation functions for 3 such quenches. Squares are the correlation points for a 1.5 K quench below the gel temperature while the circles and diamonds are for -1.25 and -1.0 K quenches. The curve labelled A was obtained soonest after the quench while that labelled G was obtained latest. The decay time of the curves provide a measure of how dynamic the nanoparticles are. Soon after the quench (A curves), the decay is relatively rapid indicating motion of small clusters of nanoparticles while long after the quench (G curves), the decay is incomplete indicating that the nanoparticle motion has largely been arrested and that the gel is nearly fully formed. The illustrations in the lower left and upper right of Fig. 12 are schematic illustrations of the microscopic state of the suspension at these two extremes of observed behavior.

This work suggests that gel formation in intermediate concentration colloidal suspensions occurs via the formation of highly favored small clusters of nanoparticles like those illustrated schematically in the lower left of Fig. 12 and then, via relatively slow diffusion, the clusters interact and form a space-spanning gel structure like that shown schematically in the upper right of Fig. 12 and complements previous work in this area [105]–[107] that reached similar conclusions but without the same measured insight into the nanoscale dynamics.

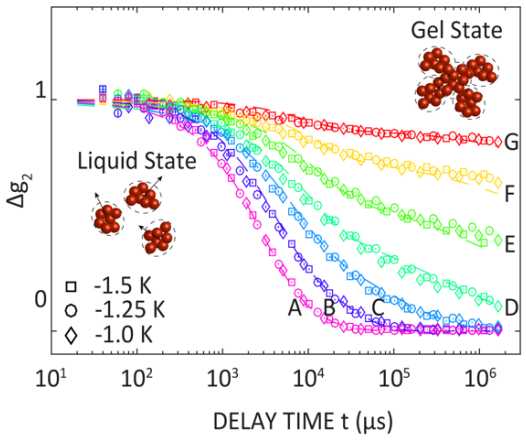

FIG. 12. Autocorrelation decay functions indicating the dynamic state of the gelling nanoparticle suspension after 3 different quenches into the gel-forming regime. Each of the curves (A–G) is comprised of data points obtained from the 3 quenches listed in the legend with the only difference being how long after the quench the same decay functions were measured. The lines through the data points are guides-to-the-eye. The microscopic structures of the gel in its liquid and gelled states are shown schematically in the lower left and upper right corners of the figure, respectively. Adapted from Zhang *et al.* [104].

VI. XPCS FOR STUDIES OF MATERIALS AGING AND FATIGUE

A. Microscopic Repeatability under External Stimuli

The short wavelength and high penetrating power of synchrotron hard x-ray beams have enabled time-resolved studies of important physical processes under various *in situ* and *in operando* conditions with nm-scale spatial resolution and sensitivity. Examples include the propagation of strain and phase boundaries within electrode nanoparticles in lithium batteries during operating cycles [108] and the formation and annihilation of serpentine striped magnetic nanodomains in epitaxial multilayer structures [95]. The performance of functional nanomaterials is often significantly affected by larger, i.e., statistically significant, ensembles of the constituents. For example, in the case of lithium batteries, the loss of repeatability of the microscopic structures of large ensembles of cathode nanoparticles after a certain number of charge/discharge cycles is associated with fatigue and can critically impact the lifetime and the performance of a working battery. For this reason, correlation

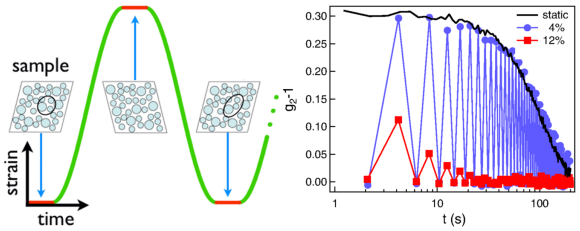

FIG. 13. Left panel: Schematic of a shear echo experiment in which speckle patterns are measured stroboscopically at the extremes of a shear cycle. Right panel: Speckle pattern correlations versus shear cycle (mapped onto time). The periodic high and low correlations correspond to data obtained at the two extremes of the shear cycle. The black line is for a quiescent sample while the blue and red points and lines are for samples sheared to the strain values listed in the inset. Figure adapted from Ref. [110].

analysis over an ensemble of microscopic states is useful. Techniques like XPCS measure the correlation of microscopic spatial disorder by calculating the average overlap of coherent x-ray scattering patterns after repeat cycles [109] and offer a powerful method for studying the microscopic repeatability of nanomaterials under various operating conditions.

A recent example of an experiment of this type was performed by M. Rogers *et al.* [110] on intermediate concentration colloidal gels in a shear-cell rheometer. The samples consisted of octadecyl-grafted silica nanoparticles dispersed in decalin with $\phi = 0.3$. Polystyrene was added to induce gelation through an entropic depletion attraction. The gel was then placed in a shear cell that was realized by two thin diamond plates where one diamond plate remains stationary and the other is moved to apply oscillatory shear. Speckle patterns were measured from the sample during repeated shear cycles of varying strain. Speckle patterns from the sheared sample were captured in a stroboscopic manner at the extremes of the shear cycle (left panel of Fig. 13). Within the linear regime where the deformation is considered to be elastic, it was found that the decorrelation over the number of cycles of shearing strain is modulated by the dynamics of the sample in the absence of shearing. Above a threshold strain that is near the yield point of the gel, the correlation over subsequent shearing cycles decreases drastically. These conclusions are illustrated in the right panel of Fig. 13. The figure shows that the decorrelation of g_2 for a quiescent sample (black line) and a gently sheared sample (blue points and line) are virtually identical while the decorrelation from a more strongly sheared sample (red points and line) decays over a much smaller number

of shear cycles (time). Detailed analysis shows a power law scaling between the rate of irreversible decorrelations per volume = $N(V) \sim V^{-\xi}$, where V is the volume, $N(V)$ is the number of events that lead to irreversible deformation and the scaling factor ξ is determined from the experimental results to be 1.56 ± 0.06. The power law found indicates a non-equilibrium critical transition in the gel at yielding.

B. Aging Behavior in Materials Probed by XPCS

Understanding how materials age is an important aspect of potentially applying them for advanced applications. XPCS is sensitive to slow changes in the exact position of constituent atoms and nanoparticles in disordered materials and therefore is well suited to studying aging properties in glassy materials. To date, XPCS work in this area has mostly focused on the aging behavior of metallic glasses and in soft solids composed of colloidal particles.

Metallic glasses, in particular, provide outstanding mechanical strength, elasticity and wear and corrosion resistance while bulk metallic glasses offer these outstanding physical properties in forms large enough for practical applications [55]. Because of their potential technological importance and because at a fundamental level understanding the glass transition remains a grand challenge, XPCS has been used to understand the aging and long-term behavior of a variety of metallic glasses. A recent highlight in this area is a combined XPCS and high energy x-ray diffraction (XRD) study to examine the dynamic and structural properties of the metallic glass $Pd_{77}Si_{16.5}Cu_{6.5}$ as a rapidly quenched sample was successively heated closer and closer to its glass transition temperature (T_g) [61]. XPCS provided sensitivity to motion at the atomic scale and XRD provided information about subtle structural changes in the glass that occur during heating. The study found that upon heating, the dynamics observed by XPCS would slow as the sample was held (aged) at a particular temperature but would speed up (and then slow again) when the hold temperature was increased. This behavior persisted until at a certain elevated temperature (but still below T_g) the aging behavior stopped and XPCS dynamics were independent of dwell time. At even higher temperatures, the short-time amplitudes of the XPCS correlation functions decrease indicating the presence of dynamics at shorter time scales that are currently too fast for XPCS to resolve. The origin of this loss of amplitude is not fully understood at this point but is believed to be related to incipient crystallization of the glass which is suggested

by the complementary XRD results. Work in this area remains challenging because of weak scattering signals that limit studies to slow dynamics and to the immediate vicinity of the first sharp diffraction peak (FSDP). Nevertheless, there have been many outstanding studies reported in this area [61]–[63], [111], [112] and this field is expected to blossom with the anticipated emergence of dramatically more coherent synchrotron light sources.

VII. CONCLUDING REMARKS AND FUTURE OPPORTUNITIES

In this review we have summarized XPCS as it applies to understanding different aspects of materials stability, formation and aging. In recent years, with advances in beamline set-ups, detectors and user-friendly software, XPCS has transformed from an x-ray-experts-only technique to a tool used by a variety of researchers in materials science and engineering related disciplines.

Despite these advances, the applicability of XPCS to various scientific problems has often been limited by available coherent flux, especially at higher x-ray energies. This situation will dramatically improve over the next 5–10 years. First, higher repetition rate FELs such as XFEL and LCLS-II will provide markedly improved time-averaged coherent flux that could be beneficial for XPCS. More exciting, in our opinion, is the dawning of multi-bend achromat (MBA) storage-rings. These so-called fourth generation storage rings (see, for example, Ref. [113] and subsequent articles in the same journal issue) will provide coherent fluxes in the hard x-ray regime 10–100$\times$ greater than today and these gains will extend well into the hard x-ray regime. MBA rings achieve their dramatic gains by replacing the relatively large dipole bending angle in third generation rings today with a series of much smaller bending angles interspersed with multipole magnets that provide focusing between the dipoles [114]. In this manner, the horizontal emittance ϵ_x is dramatically reduced, namely by $\epsilon_x \simeq E^2/N_d^3$, where E is the storage ring energy and N_d is the number of dipoles. The first storage ring of this type, MAX-IV in Sweden, is undergoing commissioning now. Most relevant to XPCS are plans to upgrade the ESRF and APS to MBA storage rings, namely ESRF-EBS (extremely brilliant source) and APS-U (upgrade). At both facilities, the XPCS capabilities will be significantly upgraded or replaced to take full advantage of the greatly increased coherent flux provided by these effectively new facilities. At APS-U, for example, the horizontal emittance is projected to change from more than 3,000 pm $\cdot$ rad

today to 42 pm · rad in the future and produce 100× or more coherent flux than is available at the APS today.

To conclude, we note that for XPCS the signal-to-noise ratio (SNR) depends linearly on the coherent flux and as the square root of the minimum accessible delay time [115]. At APS-U, with 100× more coherent flux than today and the same SNR, minimum accessible delay times 10,000× faster than today should be accessible. This will continue to expand the impact that XPCS is having on materials research.

DISCLOSURE STATEMENT

The authors are not aware of any affiliations, memberships, funding, or financial holdings that might be perceived as affecting the objectivity of this review.

ACKNOWLEDGMENTS

We have benefited from many fruitful collaborations and conversations with a great many colleagues. These include Yuriy Chushkin, Eric Dufresne, Andrei Fluerasu, Gerhard Grübel, Zhang Jiang, Robert Leheny, Anders Madsen, Simon Mochrie, Suresh Narayanan, Sunil Sinha, Michael Sprung, Mark Sutton and Jin Wang. Portions of this work were supported by the resources of the Advanced Photon Source, a U.S. Department of Energy (DOE) Office of Science User Facility operated for the DOE Office of Science by Argonne National Laboratory under Contract No. DE-AC02-06CH11357.

LITERATURE CITED

REFERENCES

[1] F. Livet, "Diffraction with a coherent x-ray beam: Dynamics and imaging," *Acta Cryst. A*, vol. 63, pp. 87–107, 2007.

[2] G. Grübel, A. Madsen, and A. Robert, "X-Ray Photon Correlation Spectroscopy," in *Soft Matter Characterization*. New York, New York: Springer Netherlands, 2008, pp. 953–995.

[3] M. Sutton, "A review of x-ray intensity fluctuation spectroscopy," *C. R. Phys.*, vol. 9, pp. 657–667, 2008.

[4] F. Livet and M. Sutton, "X-ray coherent scattering in metal physics," *C. R. Phys.*, vol. 13, pp. 23–32, 2012.

[5] S. K. Sinha, Z. Jiang, and L. B. Lurio, "X-ray photon correlation spectroscopy studies of surfaces and thin films," *Adv. Mat.*, vol. 26, pp. 7764–7785, 2014.

[6] A. Madsen, A. Fluerasu, and B. Ruta, "Structural Dynamics of Materials Probed by X-Ray Photon Correlation Spectroscopy," in *Synchrotron Light Sources and Free-Electron Lasers*. Switzerland: Springer International Publishing, 2016, pp. 1617–1641.

[7] M. Sutton, S. G. J. Mochrie, T. Greytak, S. E. Nagler, L. E. Berman, G. A. Held, and G. B. Stephenson, "Observation of speckle by diffraction with coherent x-rays," *Nature*, vol. 352, pp. 608–610, 1991.

[8] J. Miao, T. Ishikawa, I. K. Robinson, and M. M. Murnane, "Beyond crystallography: Diffractive imaging using coherent x-ray light sources," *Science*, vol. 348, no. 6234, pp. 530–535, 2015.

[9] M. Born and E. Wolf, *Principles of optics: Electromagnetic theory of propagation, interference and diffraction of light*. Oxford: Pergamon, 1980.

[10] J. W. Goodman, *Statistical Optics*. New York: Wiley, 1985.

[11] I. A. Vartanyants and A. Singer, "Coherence properties of hard x-ray synchrotron sources and x-ray free electron lasers," *New J. Phys.*, vol. 12, p. 035 004, 2010.

[12] A. R. Sandy, L. B. Lurio, S. G. J. Mochrie, A. Malik, G. B. Stephenson, J. F. Pelletier, and M. Sutton, "Design and characterization of an undulator beamline optimized for small-angle coherent x-ray scattering at the Advanced Photon Source," *J. Synchrotron Radiat.*, vol. 6, pp. 1174–1184, 1999.

[13] F. Pfeiffer, W. Zhang, and I. K. Robinson, "Coherent grazing exit x-ray scattering geometry for probing the structure of thin films," *Appl. Phys. Lett.*, vol. 84, pp. 1847–1849, 2004.

[14] D. Markowitz and L. P. Kadanoff, "Effect of impurities upon critical temperature of anisotropic superconductors," *Phys. Rev.*, vol. 131, pp. 563–575, 1963.

[15] S. B. Dierker, R. Pindak, R. M. Fleming, I. K. Robinson, and L. Berman, "X-ray photon-correlation spectroscopy study of brownian-motion of gold colloids in glycerol," *Phys. Rev. Lett.*, vol. 75, pp. 449–452, 1995.

[16] F. Zhang, A. J. Allen, L. E. Levine, L. Espinal, J. M. Antonucci, D. Skrtic, J. N. R. O'Donnell, and J. Ilavsky, "Ultra-small-angle x-ray scattering-x-ray photon correlation spectroscopy studies of incipient structural changes in amorphous calcium phosphate-based dental composites," *J. Biomed. Mat. Res. A*, vol. 100A, pp. 1293–1306, 2012.

[17] Q. Zhang, E. M. Dufresne, P. Chen, J. Park, M. P. Cosgriff, M. Yusuf, Y. Dong, D. D. Fong, H. Zhou, Z. Cai, R. J. Harder, S. J. Callori, M. Dawber, P. G. Evans, and A. R. Sandy, "Thermal fluctuations of ferroelectric nanodomains in a ferroelectric-dielectric $PbTiO_3/SrTiO_3$ superlattice," *Phys. Rev. Lett.*, vol. 118, p. 097 601, 2017.

[18] A. Barbour, A. Alatas, Y. Liu, C. Zhu, B. M. Leu, X. Zhang, A. Sandy, M. S. Pierce, X. Wang, S. W. Cheong, and H. You, "Partial glass isosymmetry transition in multiferroic hexagonal $ErMnO_3$," *Phys. Rev. B*, vol. 93, p. 054 113, 2016.

[19] A. Singer, S. K. K. Patel, V. Uhlíř, R. Kukreja, A. Ulvestad, E. M. Dufresne, A. R. Sandy, E. E. Fullerton, and O. G. Shpyrko, "Phase coexistence and pinning of charge density waves by interfaces in chromium," *Phys. Rev. B*, vol. 94, p. 174 110, 2016.

[20] O. G. Shpyrko, E. D. Isaacs, J. M. Logan, Y. J. Feng, G. Aeppli, R. Jaramillo, H. C. Kim, T. F. Rosenbaum, P. Zschack, M. Sprung, S. Narayanan, and A. R. Sandy, "Direct measurement of antiferromagnetic domain fluctuations," *Nature*, vol. 447, pp. 68–71, 2007.

[21] J. Su, A. R. Sandy, J. Mohanty, O. G. Shpyrko, and M. Sutton, "Collective pinning dynamics of charge-density waves in 1T-TaS_2," *Phys. Rev. B*, vol. 86, p. 205 105, 2012.

[22] A. Fluerasu, M. Sutton, and E. M. Dufresne, "X-ray intensity fluctuation spectroscopy studies on phase-ordering systems," *Phys. Rev. Lett.*, vol. 94, p. 055 501, 2005.

[23] C. Sanborn, K. F. Ludwig, M. C. Rogers, and M. Sutton, "Direct measurement of microstructural avalanches during the martensitic transition of cobalt using coherent x-ray scattering," *Phys. Rev. Lett.*, vol. 107, p. 015 702, 2011.

[24] F. Livet, M. Fèvre, G. Beutier, and M. Sutton, "Ordering fluctuation dynamics in $AuAgZn_2$," *Phys. Rev. B*, vol. 92, p. 094 102, 2015.

[25] M. S. Pierce, K. C. Chang, D. Hennessy, V. Komanicky, M. Sprung, A. Sandy, and H. You, "Surface x-ray speckles: Coherent surface diffraction from Au(001)," *Phys. Rev. Lett.*, vol. 103, p. 165 501, 2009.

[26] M. S. Pierce, D. C. Hennessy, K. C. Chang, V. Komanicky, J. Strzalka, A. Sandy, A. Barbour, and H. You, "Persistent oscillations of x-ray speckles: Pt(001) step flow," *Appl. Phys. Lett.*, vol. 99, p. 121 910, 2011.

[27] M. S. Pierce, V. Komanicky, A. Barbour, D. C. Hennessy, J. D. Suc, A. Sandy, C. Zhu, and H. You, "In-situ coherent x-ray scattering and scanning tunneling microscopy studies of hexagonally reconstructed Au(001) in electrolytes," in *Electrocatalysis 5*, ser. ECS transactions. 2011, vol. 35, pp. 71–81.

[28] M. S. Pierce, V. Komanicky, A. Barbour, D. C. Hennessy, C. H. Zhu, A. Sandy, and H. You, "Dynamics of the Au(001) surface in electrolytes: In situ coherent x-ray scattering," *Phys. Rev. B*, vol. 86, p. 085 410, 2012.

[29] M. S. Pierce, A. Barbour, V. Komanicky, D. Hennessy, and H. You, "Coherent x-ray scattering experiments of Pt(001) surface dynamics near a roughening transition," *Phys. Rev. B*, vol. 86, p. 184 108, 2012.

[30] R. M. Karl, A. Barbour, V. Komanicky, C. H. Zhu, A. Sandy, M. S. Pierce, and H. You, "Charge-induced equilibrium dynamics and structure at the Ag(001)-electrolyte interface," *Phys. Chem. Chem. Phys.*, vol. 17, pp. 16 682–16 687, 2015.

[31] R. A. Narayanan, P. Thiyagarajan, S. Lewis, A. Bansal, L. S. Schadler, and L. B. Lurio, "Dynamics and internal stress at the nanoscale related to unique thermomechanical behavior in polymer nanocomposites," *Phys. Rev. Lett.*, vol. 97, p. 075 505, 2006.

[32] S. Narayanan, D. R. Lee, A. Hagman, X. F. Li, and J. Wang, "Particle dynamics in polymer-metal nanocomposite thin films on nanometer-length scales," *Phys. Rev. Lett.*, vol. 98, p. 185 506, 2007.

[33] A. K. Kandar, S. Srivastava, J. K. Basu, M. K. Mukhopadhyay, S. Seifert, and S. Narayanan, "Unusual dynamical arrest in polymer grafted nanoparticles," *J. Chem. Phys.*, vol. 130, p. 121 102, 2009.

[34] S. Srivastava, A. K. Kandar, J. K. Basu, M. K. Mukhopadhyay, L. B. Lurio, S. Narayanan, and S. K. Sinha, "Complex dynamics in polymer nanocomposites," *Phys. Rev. E*, vol. 79, p. 021 408, 2009.

[35] S. Srivastava, S. Chandran, A. K. Kandar, C. K. Sarika, J. K. Basu, S. Narayanan, and A. Sandy, "Communication: Unusual dynamics of hybrid nanoparticles and their binary mixtures," *J. Chem. Phys.*, vol. 133, p. 151 105, 2010.

[36] M. Sikorski, A. R. Sandy, and S. Narayanan, "Depletion-induced structure and dynamics in bimodal colloidal suspensions," *Phys. Rev. Lett.*, vol. 106, p. 188 301, 2011.

[37] H. Guo, G. Bourret, R. B. Lennox, M. Sutton, J. L. Harden, and R. L. Leheny, "Entanglement-controlled subdiffusion of nanoparticles within concentrated polymer solutions," *Phys. Rev. Lett.*, vol. 109, p. 055 901, 2012.

[38] D. Kim, S. Srivastava, S. Narayanan, and L. A. Archer, "Polymer nanocomposites: Polymer and particle dynamics," *Soft Matter*, vol. 8, pp. 10 813–10 818, 2012.

[39] S. Srivastava, L. A. Archer, and S. Narayanan, "Structure and transport anomalies in soft colloids," *Phys. Rev. Lett.*, vol. 110, p. 148 302, 2013.

[40] W. S. Jang, P. Koo, K. Bryson, S. Narayanan, A. Sandy, T. P. Russell, and S. G. Mochrie, "Dynamics of cadmium sulfide nanoparticles within polystyrene melts," *Macromolecules*, vol. 47, pp. 6483–6490, 2014.

[41] A. Agrawal, H.-Y. Yu, S. Srivastava, S. Choudhury, S. Narayanan, and L. A. Archer, "Dynamics and yielding of binary self-suspended nanoparticle fluids," *Soft Matter*, vol. 11, pp. 5224–5234, 2015.

[42] M. Ranka, N. Varkey, S. Ramakrishnan, and C. F. Zukoski, "Impact of small changes in particle surface chemistry for unentangled polymer nanocomposites," *Soft Matter*, vol. 11, pp. 1634–1645, 2015.

[43] S. Srivastava, P. Agarwal, R. Mangal, D. L. Koch, S. Narayanan, and L. A. Archer, "Hyperdiffusive dynamics in newtonian nanoparticle fluids," *ACS Macro Lett.*, vol. 4, pp. 1149–1153, 2015.

[44] A. Grein-Iankovski, I. C. Riegel-Vidotti, F. F. Simas-Tosin, S. Narayanan, R. L. Leheny, and A. R. Sandy, "Exploring the relationship between nanoscale dynamics and macroscopic rheology in natural polymer gums," *Soft Matter*, vol. 12, pp. 9321–9329, 2016.

[45] W. S. Jang, P. Koo, K. Bryson, S. Narayanan, A. R. Sandy, T. P. Russell, and S. G. Mochrie, "The static structure and dynamics of cadmium sulfide nanoparticles within poly(styrene-block-isoprene) diblock copolymer melts," *Macromol. Chem. Phys.*, vol. 217, pp. 591–598, 2016.

[46] S. Q. Liu, E. Senses, Y. Jiao, S. Narayanan, and P. Akcora, "Structure and entanglement factors on dynamics of polymer-grafted nanoparticles," *ACS Macro Lett.*, vol. 5, pp. 569–573, 2016.

[47] R. Mangal, S. Srivastava, S. Narayanan, and L. A. Archer, "Size-dependent particle dynamics in entangled polymer nanocomposites," *Langmuir*, vol. 32, pp. 596–603, 2016.

[48] R. Poling-Skutvik, K. I. S. Mongcopa, A. Faraone, S. Narayanan, J. C. Conrad, and R. Krishnamoorti, "Structure and dynamics of interacting nanoparticles in semidilute polymer solutions," *Macromolecules*, vol. 49, pp. 6568–6577, 2016.

[49] S. Srivastava, S. Kishore, S. Narayanan, A. R. Sandy, and S. R. Bhatia, "Multiple dynamic regimes in colloid-polymer dispersions: New insight using x-ray photon correlation spectroscopy," *J. Polym. Sci. B Polym. Phys.*, vol. 54, pp. 752–760, 2016.

[50] J. Lee, A. Grein-Iankovski, S. Narayanan, and R. L. Leheny, "Nanorod mobility within entangled wormlike micelle solutions," *Macromolecules*, vol. 50, pp. 406–415, 2017.

[51] E. Senses, S. M. Ansar, C. L. Kitchens, Y. Mao, S. Narayanan, B. Natarajan, and A. Faraone, "Small particle driven chain disentanglements in polymer nanocomposites," *Phys. Rev. Lett.*, vol. 118, p. 147 801, 2017.

[52] C. Broennimann, E. F. Eikenberry, B. Henrich, R. Horisberger, G. Huelsen, E. Pohl, B. Schmitt, C. Schulze-Briese, M. Suzuki, T. Tomizaki, H. Toyokawa, and A. Wagner, "The PILATUS 1M detector," *J. Synchrotron Radiat.*, vol. 13, pp. 120–130, 2006.

[53] I. Johnson, A. Bergamaschi, J. Buitenhuis, R. Dinapoli, D. Greiffenberg, B. Henrich, T. Ikonen, G. Meier, A. Menzel, A. Mozzanica, V. Radicci, D. K. Satapathy, B. Schmitt, and X. Shi, "Capturing dynamics with Eiger, a fast-framing x-ray detector," *J. Synchrotron Radiat.*, vol. 19, pp. 1001–1005, 2012.

[54] D. Pennicard, S. Lange, S. Smoljanin, H. Hirsemann, and H. Graafsma, "LAMBDA—Large Area Medipix3-Based Detector Array," *J. Instr.*, vol. 7, p. C11009, 2012.

[55] M. Chen, "A brief overview of bulk metallic glasses," *NPG Asia Materials*, vol. 3, pp. 82–90, Sep. 2011.

[56] J. Schroers, "Bulk Metallic Glasses," *Physics Today*, vol. 66, pp. 32–7, 2013.

[57] C. J. Byrne and M. Eldrup, "Bulk Metallic Glasses," *Science*, vol. 321, p. 502, Jul. 2008.

[58] L.-M. Martinez and C. A. Angell, "A thermodynamic connection to the fragility of glass-forming liquids," *Nature*, vol. 410, pp. 663–667, 2001.

[59] L. Berthier, G. Biroli, J.-P. Bouchaud, L. Cipelletti, D. E. Masri, D. L'Hôte, F. Ladieu, and M. Pierno, "Direct experimental evidence of a growing length scale accompanying the glass transition," *Science*, vol. 310, pp. 1797–1800, 2005.

[60] B. Ruta, G. Baldi, Y. Chushkin, B. Ruffle, L. Cristofolini, A. Fontana, M. Zanatta, and F. Nazzani, "Revealing the fast atomic motion of network glasses," *Nat. Comm.*, vol. 5, p. 3939, May 2014.

[61] V. M. Giordano and B. Ruta, "Unveiling the structural arrangements responsible for the atomic dynamics in metallic glasses during physical aging," *Nat. Comm.*, vol. 7, pp. 1–8, Jan. 2016.

[62] B. Ruta, Y. Chushkin, G. Monaco, L. Cipelletti, E. Pineda, P. Bruna, V. M. Giordano, and M. Gonzalez-Silveira, "Atomic-scale relaxation dynamics and aging in a metallic glass probed by x-ray photon correlation spectroscopy," *Phys. Rev. Lett.*, vol. 109, p. 165 701, 2012.

[63] Z. Evenson, B. Ruta, S. Hechler, M. Stolpe, E. Pineda, I. Gallino, and R. Busch, "X-ray photon correlation spectroscopy reveals intermittent aging dynamics in a metallic glass," *Phys. Rev. Lett.*, vol. 115, p. 5, 2015.

[64] T. Thurn-Albrecht, W. Steffen, A. Patkowski, G. Meier, E. W. Fischer, G. Grübel, and D. L. Abernathy, "Photon correlation spectroscopy of colloidal palladium using a coherent x-ray beam," *Phys. Rev. Lett.*, vol. 77, pp. 5437–5440, 1996.

[65] J. Lal, D. Abernathy, L. Auvray, O. Diat, and G. Grübel, "Dynamics and correlations in magnetic colloidal systems studied by x-ray photon correlation spectroscopy," *Eur. Phys. J. E*, vol. 4, pp. 263–271, 2001.

[66] T. Autenrieth, A. Robert, J. Wagner, and G. Grübel, "The dynamic behavior of magnetic colloids in suspension," *J. Appl. Cryst.*, vol. 40, S250–S253, 2007.

[67] A. Fluerasu, A. Moussaïd, A. Madsen, and A. Schofield, "Slow dynamics and aging in colloidal gels studied by x-ray photon correlation spectroscopy," *Phys. Rev. E*, vol. 76, 010401(R), 2007.

[68] V. Trappe, E. Pitard, L. Ramos, A. Robert, H. Bissig, and L. Cipelletti, "Investigation of q-dependent dynamical heterogeneity in a colloidal gel by x-ray photon correlation spectroscopy," *Phys. Rev. E*, vol. 76, p. 051 404, 2007.

[69] A. Robert, J. Wagner, W. Haertl, T. Autenrieth, and G. Grübel, "Dynamics in dense suspensions of charge-stabilized colloidal particles," *Eur. Phys. J. E*, vol. 25, pp. 77–81, 2008.

[70] H. Y. Guo, S. Ramakrishnan, J. L. Harden, and R. L. Leheny, "Connecting nanoscale motion and rheology of gel-forming colloidal suspensions," *Phys. Rev. E*, vol. 81, 050401(R), 2010.

[71] H. Guo, S. Ramakrishnan, J. L. Harden, and R. L. Leheny, "Gel formation and aging in weakly attractive nanocolloid suspensions at intermediate concentrations," *J. Chem. Phys.*, vol. 135, p. 154 903, 2011.

[72] M. Spannuth, S. G. J. Mochrie, S. S. L. Peppin, and J. S. Wettlaufer, "Dynamics of colloidal particles in ice," *J. Chem. Phys.*, vol. 135, 2011.

[73] D. Orsi, A. Fluerasu, A. Moussaid, F. Zontone, L. Cristofolini, and A. Madsen, "Dynamics in dense hard-sphere colloidal suspensions," *Phys. Rev. E*, vol. 85, p. 011 402, 2012.

[74] F. Westermeier, B. Fischer, W. Roseker, G. Grübel, G. Naegele, and M. Heinen, "Structure and short-time dynamics in concentrated suspensions of charged colloids," *J. Chem. Phys.*, vol. 137, p. 114 504, 2012.

[75] R. Angelini, L. Zulian, A. Fluerasu, A. Madsen, G. Ruocco, and B. Ruzicka, "Dichotomic aging behaviour in a colloidal glass," *Soft Matter*, vol. 9, pp. 10 955–10 959, 2013.

[76] F. Zhang, A. J. Allen, L. E. Levine, J. Ilavsky, and G. G. Long, "Structure and dynamics studies of concentrated micrometer-sized colloidal suspensions," *Langmuir*, vol. 29, pp. 1379–1387, 2013.

[77] R. Angelini, A. Madsen, A. Fluerasu, G. Ruocco, and B. Ruzicka, "Aging behavior of the localization length in a colloidal glass," *Colloids Surf. A Physicochem. Eng. Asp.*, vol. 460, pp. 118–122, 2014.

[78] R. Angelini, E. Zaccarelli, F. A. D. Marques, M. Sztucki, A. Fluerasu, G. Ruocco, and B. Ruzicka, "Glass-glass transition during aging of a colloidal clay," *Nat. Comm.*, vol. 5, p. 4049, 2014.

[79] F. A. D. Marques, R. Angelini, E. Zaccarelli, B. Farago, B. Ruta, G. Ruocco, and B. Ruzicka, "Structural and microscopic relaxations in a colloidal glass," *Soft Matter*, vol. 11, pp. 466–471, 2015.

[80] P. N. Pusey, "Colloidal suspensions," in *Liquids, Freezing and the Glass Transition*. Amsterdam: Elsevier, 1991, ch. 10, pp. 763–942.

[81] P.-G. de Gennes, *Scaling Concepts in Polymer Physics*. Ithaca, NY: Cornell University Press, 1979.

[82] G. L. Hunter and E. R. Weeks, "The physics of the colloidal glass transition," *Rep. Prog. Phys.*, vol. 75, p. 066 501, 2012.

[83] D. Lumma, L. B. Lurio, M. A. Borthwick, P. Falus, and S. G. J. Mochrie, "Structure and dynamics of concentrated dispersions of polystyrene latex spheres in glycerol: Static and dynamic x-ray scattering," *Phys. Rev. E*, vol. 62, pp. 8258–8269, 2000.

[84] D. Beysens and T. Narayanan, "Wetting-induced aggregation of colloids," *Journal of Statistical Physics*, vol. 95, pp. 997–1008, 1999.

[85] D. Pontoni, T. Narayanan, J. M. Petit, G. Grübel, and D. Beysens, "Microstructure and dynamics near an attractive colloidal glass transition," *Phys. Rev. Lett.*, vol. 90, p. 188 301, 2003.

[86] X. H. Lu, S. G. J. Mochrie, S. Narayanan, A. R. Sandy, and M. Sprung, "How a liquid becomes a glass both on cooling and on heating," *Phys. Rev. Lett.*, vol. 100, p. 045 701, 2008.

[87] ——, "Temperature-dependent structural arrest of silica colloids in a water-lutidine binary mixture," *Soft Matter*, vol. 6, pp. 6160–6177, 2010.

[88] P. Falus, M. A. Borthwick, and S. G. J. Mochrie, "Fast CCD camera for x-ray photon correlation spectroscopy and time-resolved x-ray scattering and imaging," *Rev. Sci. Instrum.*, vol. 75, pp. 4383–4400, 2004.

[89] W. Götze and M. Sperl, "Logarithmic relaxation in glass-forming systems," *Phys. Rev. E*, vol. 66, p. 011 405, 2002.

[90] L. Cipelletti, S. Manley, R. C. Ball, and D. A. Weitz, "Universal aging features in the restructuring of fractal colloidal gels," *Physical Review Letters*, vol. 84, no. 10, pp. 2275–2278, 2000.

[91] J. P. Bouchaud and E. Pitard, "Anomalous dynamical light scattering in soft glassy gels," *European Physical Journal E*, vol. 6, pp. 231–236, 2001.

[92] P. Akcora, S. K. Kumar, J. Moll, S. Lewis, L. S. Schadler, Y. Li, B. C. Benicewicz, A. Sandy, S. Narayanan, J. Illavsky, P. Thiyagarajan, R. H. Colby, and J. F. Douglas, ""gel-like" mechanical reinforcement in polymer nanocomposite melts," *Macromolecules*, vol. 43, pp. 1003–1010, 2010.

[93] X. M. Chen, V. Thampy, C. Mazzoli, A. M. Barbour, H. Miao, G. D. Gu, Y. Cao, J. M. Tranquada, M. P. M. Dean, and S. B. Wilkins, "Remarkable stability of charge density wave order in $La_{1.875}Ba_{0.125}CuO_4$," *Phys. Rev. Lett.*, vol. 117, p. 6, 2016.

[94] P. G. Evans, E. D. Isaacs, G. Aeppli, Z. Cai, and B. Lai, "X-ray microdiffraction images of antiferromagnetic domain evolution in chromium," *Science*, vol. 295, no. 5557, pp. 1042–5, 2002.

[95] A. Tripathi, J. Mohanty, S. H. Dietze, O. G. Shpyrko, E. Shipton, E. E. Fullerton, S. S. Kim, and I. McNulty, "Dichroic coherent diffractive imaging," *Proc. Natl. Acad. Sci. USA*, vol. 108, pp. 13 393–13 398, 2011.

[96] S. S. Parkin, M. Hayashi, and L. Thomas, "Magnetic domain-wall racetrack memory," *Science*, vol. 320, pp. 190–194, 2008.

[97] D. A. Allwood, G. Xiong, C. C. Faulkner, D. Atkinson, D. Petit, and R. P. Cowburn, "Magnetic domain-wall logic," *Science*, vol. 309, pp. 1688–92, 2005.

[98] A. Malik, A. R. Sandy, L. B. Lurio, G. B. Stephenson, S. G. J. Mochrie, I. McNulty, and M. Sutton, "Coherent x-ray study of fluctuations during domain coarsening," *Phys. Rev. Lett.*, vol. 81, pp. 5832–5835, 1998.

[99] O. Bikondoa, "On the use of two-time correlation functions for X-ray photon correlation spectroscopy data analysis," *J. Appl. Cryst.*, vol. 50, pp. 357–368, 2017.

[100] D. Bonn, H. Kellay, H. Tanaka, G. Wegdam, and J. Meunier, "Laponite: What is the difference between a gel and a glass?" *Langmuir*, vol. 15, no. 22, pp. 7534–7536, 1999.

[101] E. Zaccarelli, "Colloidal gels: Equilibrium and non-equilibrium routes," *J. Phys.: Condens. Matter*, vol. 19, p. 323 101, 2007.

[102] Q. Zhang, E. M. Dufresne, P. Grybos, P. Kmon, P. Maj, S. Narayanan, G. W. Deptuch, R. Szczygiel, and A. Sandy, "Submillisecond x-ray photon correlation spectroscopy from a pixel array detector with fast dual gating and no readout dead-time," *J. Synchrotron Radiat.*, vol. 23, pp. 679–684, 2016.

[103] P. Grybos, P. Kmon, P. Maj, and R. Szczygiel, "32k channel readout IC for single photon counting pixel detectors with 75 μm pitch, dead time of 85 ns, 9 e^- offset spread and 2% rms gain spread," *IEEE T. Nucl. Sci.*, vol. 63, pp. 1155–1161, 2016.

[104] Q. Zhang, D. Bahadur, E. M. Dufresne, P. Grybos, P. Kmon, R. L. Leheny, P. Maj, S. Narayanan, R. Szczygiel, S. Ramakrishnan, and A. Sandy, "Dynamic scaling of colloidal gel formation at intermediate concentrations," *Phys. Rev. Lett.*, vol. 119, p. 178 006, 2017.

[105] S. Ramakrishnan, Y. L. Chen, K. S. Schweizer, and C. F. Zukoski, "Elasticity and clustering in concentrated depletion gels," *Phys. Rev. E.*, vol. 70, p. 040 401, 2004.

[106] R. N. Zia, B. J. Landrum, and W. B. Russel, "A micro-mechanical study of coarsening and rheology of colloidal gels: Cage building, cage hopping, and smoluchowski's ratchet," *J. Rheol.*, vol. 58, no. 5, pp. 1121–1157, 2014.

[107] Z. Varga, G. Wang, and J. Swan, "The hydrodynamics of colloidal gelation," *Soft Matter*, vol. 11, no. 46, pp. 9009–9019, 2015.

[108] A. Ulvestad, A. Singer, J. N. Clark, H. M. Cho, J. W. Kim, R. Harder, J. Maser, Y. S. Meng, and O. G. Shpyrko, "Topological defect dynamics in operando battery nanoparticles," *Science*, vol. 348, pp. 1344–1347, 2015.

[109] M. S. Pierce, R. G. Moore, L. B. Sorensen, S. D. Kevan, O. Hellwig, E. E. Fullerton, and J. B. Kortright, "Quasistatic x-ray speckle metrology of microscopic magnetic return-point memory," *Phys. Rev. Lett.*, vol. 90, p. 175 502, 2003.

[110] M. C. Rogers, K. Chen, L. Andrzejewski, S. Narayanan, S. Ramakrishnan, R. L. Leheny, and J. L. Harden, "Echoes in x-ray speckles track nanometer-scale plastic events in colloidal gels under shear," *Phys. Rev. E*, vol. 90, p. 062 310, 2014.

[111] B. Ruta, G. Baldi, G. Monaco, and Y. Chushkin, "Compressed correlation functions and fast aging dynamics in metallic glasses," *J. Chem. Phys.*, vol. 138, p. 6, 2013.

[112] Z. Evenson, A. Payes-Playa, Y. Chushkin, M. di Michiel, E. Pineda, and B. Ruta, "Comparing the atomic and macroscopic aging dynamics in an amorphous and partially crystalline $Zr_{44}Ti_{11}Ni_{10}Cu_{10}Be_{25}$ bulk metallic glass," *Journal of Materials Research*, vol. 32, pp. 2014–2021, 2017.

[113] M. Eriksson, J. F. van der Veen, and C. Quitmann, "Diffraction-limited storage rings – a window to the science of tomorrow," *J. of Synchrotron Radiat.*, vol. 21, pp. 837–842, 2014.

[114] R. Hettel, "DLSR design and plans: an international overview," *J. Synchrotron Radiat.*, vol. 21, pp. 843–855, 2014.

[115] E. Jakeman, in *Photon Correlation and Light Beating Spectroscopy*, H. Z. Cummins and E. R. Pike, Eds. New York: Plenum, 1973, pp. 75–149.